arXiv:1012.0227v2 [cond-mat.mes-hall] 11 Jan 2011

Polytypic nanowhiskers: electronic properties in the vicinity of the band edges

Faria Junior, P. E. and Sipahi, G. M.
Instituto de Física de São Carlos, USP, São Carlos, SP, Brazil
(ΩDated: February 16, 2022)

The increasing interest of nanowhiskers for technological applications has led to the observation of the zinc-blend/wurtzite polytypism. Polytypic nanowhiskers could also play, by their characteristics, an important role on the design of optical and electronic devices. In this work we propose a theoretical model to calculate the electronic properties of polytypic zinc-blend/wurtzite structure in the vicinity of the band edges. Our formulation is based on the $\vec{k}\cdot\vec{p}$ method connecting the irreducible representations in the interface of the two different crystalline phases by group theory arguments. Analyzing the composition of the states in the Γ point and the overlap integrals of the envelope functions we predict energy transitions that agree with experimental photoluminescence spectra.

INTRODUCTION

Recently an increasing number of papers have reported high quality and control growth of nanowires and nanowhiskers (NWs) of III-V compounds such as InP, InAs, GaAs and GaP [1–7]. Nanoelectronics, nanophotonics and solar cells are some of the technological applications for these nanostructures like described in the references above.

Vapor-liquid-solid (VLS) method [8] was used, in 1964, by Wagner and Ellis to grew a silicon whisker. Since then, other methods like molecular beam epitaxy (MBE) and metal organic vapor phase epitaxy (MOVPE) have also been applied to the growth of NWs. These techniques allow the fabrication of homo and heterostructures in both axial and radial directions opening new opportunities to engineering novel device applications.

A heterostructure is composed by assembling different materials side-by-side along a growth direction. The homostructure is a similar concept, however, it is not the kind of material that is different but its crystalline structure. This effect is also known as polytypism and have been observed in NWs structures of several III-V compounds.

Under standard temperature and pressure conditions, the III-V compounds have as the bulk stable phase the zinc-blend (ZB) structure, exception made for the nitrides that have the wurtzite (WZ) structure as the most stable phase. However, reducing the dimensions to the nanoscale level such as in these NWs, the WZ phase has been observed for non-nitride III-V compounds. The natural explanation to this behavior is the small formation energy difference between the two crystal structures.

The phase alternation creates ZB and WZ regions along the growth direction affecting the NWs optical and electronic properties, generating new forms of band offsets and electronic minibands that can be explored to produce new kinds of applications.

The WZ/ZB polytypism in III-V compounds can make a type II homostructure characterized by a staggered band-edge lineup, i. e., the charge carriers are spatially separated: the electrons will be concentrated in the ZB region while the holes will be in the WZ region. A summary of NWs growth, properties and applications was made by Dubrovskii *et al.* [9].

From the theoretical point of view, the literature about these III-V NW structures, is focused in growth stability, surface energies and formation of polytypism [10–16]. Only recently theoretical calculations of the electronic properties in the band edges have been done for such structures [17]. None has been done in the vicinity of the band edges.

The polytypism was investigated in a paper of Murayama and Nakayama [18] by *ab initio* calculations of the band offsets in WZ/ZB interfaces. A useful schematics of the correspondence between the symmetry of the states of the WZ and ZB structures has been presented in the same article.

The aim of this study is to propose a theoretical model based on group theory arguments and the $\vec{k}\cdot\vec{p}$ method to calculate the electronic band structure in the vicinity of the band edges and envelope functions of a WZ/ZB/WZ homostructure for indium phosphide (InP). The effective mass parameters for the WZ bulk phase of InP were extracted from a paper by Pryor and De [19] that predicted the band structures of some III-V bulk compounds in the WZ phase (phosphides, arsenides and antimonides). The ZB parameters are extracted from Vurgaftman *et al.* [20].

The formulation of a theoretical model for this new kind of nanostructures can lead to band gap engineering and novel electronic a and also work as a guide for the crystal growth community.

THEORETICAL MODEL

The existence two different crystal phases in a single whisker, can be explained by a simple joint analysis of the ZB and WZ crystal structures. Looking into ZB along the [111] direction and to WZ along the [0001] direction, one can found a noticeable similarity. Both can be described as stacked hexagonal layers. In fact, the ZB structure has

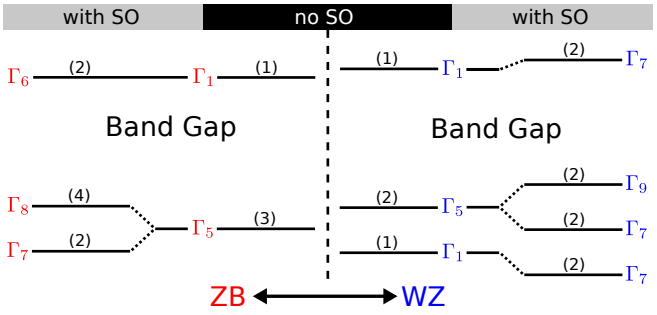


Figure 1. Γ point symmetry for the two crystal structures. The numbers in parentheses are the degeneracy of the irreducible representation. This figure was adapted form [18].

three layers in the stacking sequence (ABCABC) while the WZ structure has only two (ABAB). So, a stacking fault in WZ becomes a single segment of ZB and two sequential twin planes in ZB form a single segment of WZ [4].

An important difference between the two structures is the crystal field energy present in the WZ structure that defines the top of the valence band, neglecting spin, as a composition of two different bands, a non-degenerate and a bidegenerate bands. In ZB, the top of valence band is composed by a three-degenerate band. This difference in the energy bands between the two structures can be seen schematically for the Γ point in figure 1, with and without the spin-orbit interaction.

To calculate the band structure of a polytypic NW based in the $\vec{k}\cdot\vec{p}$ matrix formalism, it is necessary to understand the differences between the two crystal structures in the reciprocal lattice or, more precisely, what happens with the high-symmetry points in the ZB first Brillouin zone when we are dealing with the [111] growth direction and how they can be related to the WZ ones.

Looking through the [111] axis in figure 2a one can see that the L point of ZB structure is projected in the Γ point. Since the number of atoms in the primitive unit cell for WZ is twice the number in ZB, there are more states in the Γ point of WZ. This correspondence is done by assigning Γ and L points of the ZB to the Γ point of WZ. This compatibility can be seen in the energy diagram presented by Murayama and Nakayama [18], that relates the irreducible representations of the ZB Γ and L points to the WZ Γ point. This energy diagram provides the essential insight for our method since we are going to relate $\vec{k}\cdot\vec{p}$ matrices developed with irreducible representations belonging to different crystal structures.

The usual $\vec{k}\cdot\vec{p}$ matrix formulation is constructed in the vicinity of the Γ point for ZB and WZ structures [21, 22] considering the first three valence bands and the first conduction band, represented by a 4×4 matrix. When the spin-orbit interaction is included this number is multiplied by 2, resulting in a 8×8 matrix. These bands are exactly the ones presented in figure 1, and represent

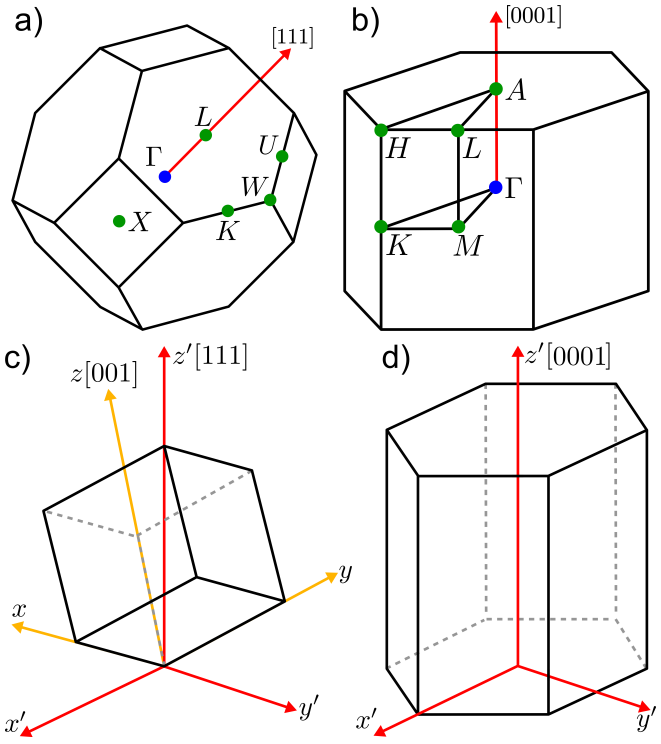


Figure 2. (a) ZB and (b) WZ first Brillouin zones. The arrows (red online) represent the growth directions. (c) ZB conventional unit cell with two different coordinate systems. (d) WZ conventional unit cell with its common coordinate system. The [111] growth direction for ZB structure passes along the main diagonal of the cube and is represented in the primed coordinate system.

a smaller set of the states first presented by Murayama and Nakamura [18]. Analyzing this, one may notice that, in the present method the irreducible representations of ZB [111] belong only to the Γ point and no irreducible representation of the L point will appear in the formulation.

Another subject, asides the symmetry correspondence, must be pointed out: the $\vec{k}\cdot\vec{p}$ matrix for the ZB structure is developed for the cubic main axes, which are the [100], [010] or [001] growth direction. This implies that the definition of the x, y, z coordinate system defines the matrix representations of the symmetry operations used to calculate the matrix elements in the $\vec{k}\cdot\vec{p}$ formulation. Changing the coordinate system to x', y', z', which is the coordinate system of the WZ Hamiltonian, will enable us to relate the ZB and WZ matrices.

We can either recalculate the matrix representations of the symmetry operations and develop the ZB $\vec{k}\cdot\vec{p}$ matrix or use the rotation matrices presented in the paper of Park and Chuang [23] to transform the ZB $\vec{k}\cdot\vec{p}$ Hamiltonian in the x, y, z to the x', y', z' coordinate system.

The basis, $\{|c_l\rangle\}$, in the prime coordinate system is defined as (from this point on, the prime will be dropped out of the notation):

$$
\begin{aligned}
|c_1\rangle &= -\frac{1}{\sqrt{2}}\,|(X+iY)\uparrow\rangle \\
|c_2\rangle &= \frac{1}{\sqrt{2}}\,|(X-iY)\uparrow\rangle \\
|c_3\rangle &= |Z\uparrow\rangle \\
|c_4\rangle &= \frac{1}{\sqrt{2}}\,|(X-iY)\downarrow\rangle \\
|c_5\rangle &= -\frac{1}{\sqrt{2}}\,|(X+iY)\downarrow\rangle \\
|c_6\rangle &= |Z\downarrow\rangle \\
|c_7\rangle &= i\,|S\uparrow\rangle \\
|c_8\rangle &= i\,|S\downarrow\rangle
\end{aligned} \tag{1}
$$

which is convenient to describe the WZ Hamiltonian.

Since we are not treating the interband interaction explicit in the matrix, the conduction band have a parabolic form for both crystals and is not affected by the rotation, reading as

$$
E_c(\vec{k}) = E_g + E_{VBM} + \frac{\hbar^2}{2m_e^{\parallel}}k_z^2 + \frac{\hbar^2}{2m_e^{\perp}}\left(k_x^2+k_y^2\right) \tag{2}
$$

where E_g is the gap energy, E_{VBM} is the energy of the top valence band and for the ZB structure the electron effective masses are the same $m_e^{\parallel} = m_e^{\perp}$.

Applying the rotation matrices to the valence band ZB Hamiltonian we obtain a common matrix for the two structures:

$$
H_V = \begin{bmatrix}
F & -K^* & -H^* & 0 & 0 & 0 \\
-K & G & H & 0 & 0 & \Delta \\
-H & H^* & \lambda & 0 & \Delta & 0 \\
0 & 0 & 0 & F & -K & H \\
0 & 0 & \Delta & -K^* & G & -H^* \\
0 & \Delta & 0 & H^* & -H & \lambda
\end{bmatrix} \tag{3}
$$

The matrix terms are defined as:

$$
\begin{aligned}
F &= \Delta_1 + \Delta_2 + \lambda + \theta \\
G &= \Delta_1 - \Delta_2 + \lambda + \theta \\
\lambda &= A_1 k_z^2 + A_2\left(k_x^2+k_y^2\right) \\
\theta &= A_3 k_z^2 + A_4\left(k_x^2+k_y^2\right) \\
K &= A_5 k_+^2 + 2\sqrt{2}A_z k_- k_z \\
H &= A_6 k_+ k_z + A_z k_-^2 \\
\Delta &= \sqrt{2}\Delta_3
\end{aligned} \tag{4}
$$

where $k_\pm = k_x \pm i k_y$.

The only difference from the usual WZ formulation is the inclusion of a new parameter, A_z, that takes into account the reorientation of the ZB growth axis.

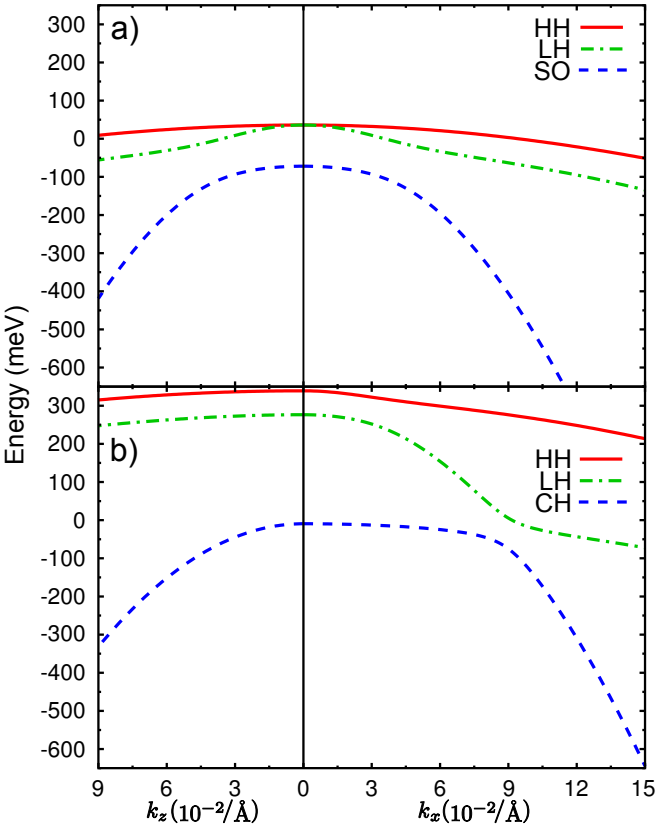


Figure 3. (a) Bulk ZB valence band structure along the [111] direction. (b) Bulk WZ valence band structure reproducing results in [19] along the [0001] growth direction. Both valence band structures were plotted for 20% of the first Brillouin Zone in k_x and k_z directions. Without spin-orbit the (x, y, z) coordinates belong to the same irreducible representation for ZB structure and then we can see that the band structure is isotropic in k_x and k_z directions. In WZ structure (x, y) and (z) coordinates belong to different irreducible representations making the band structure anisotropic in k_x and k_z directions.

The $A_i (i = 1, ..., 6, z)$, and $\Delta_i (i = 1, 2, 3)$ WZ parameters can be related to the $\gamma_i (i = 1, 2, 3)$ and Δ_{SO} ZB parameters comparing the ZB rotated matrix to the WZ matrix.

In this work we will assume the WZ as ideal and therefore the lattice parameters will considered the same as ZB. As a consequence, strain effects will not be taken into account.

RESULTS AND DISCUSSION

We first apply our model for bulk ZB and WZ InP to check the reliability of the matrix for both crystal structures. This initial investigation is useful to fit the effective mass parameters and to understand the valence band states in the band edge since now we are dealing with different basis states for the ZB matrix.

Energy	Set of states 1	Set of states 2
E_1	$\|c_1\rangle$	$\|c_4\rangle$
E_2	$\alpha\|c_2\rangle + \beta\|c_6\rangle$	$\beta\|c_3\rangle + \alpha\|c_5\rangle$
E_3	$\beta\|c_2\rangle - \alpha\|c_6\rangle$	$-\alpha\|c_3\rangle + \beta\|c_5\rangle$

Table I. The valence band energies and the respective eigenstates at the Γ point.

The ZB parameters were obtained from Ref. [20] and the WZ parameters were derived using the effective masses presented in Ref. [19]. Since in our model there is no explicit interband interaction only the valence band is presented in figure 3 for the bulk form of both crystal structures.

The usual identification of the bands were used for ZB while in WZ we had to analyze the composition of the states in the Γ point. Table I summarizes the energies and states compositions in the Γ point that helps us to identify the WZ states.

The energies and the α and β coefficients are given by [22]:

$$E_1 = \Delta_1 + \Delta_2 \tag{5}$$

$$E_2 = \frac{\Delta_1 - \Delta_2}{2} + \sqrt{\left(\frac{\Delta_1 - \Delta_2}{2}\right)^2 + 2\Delta_3^2} \tag{6}$$

$$E_3 = \frac{\Delta_1 - \Delta_2}{2} - \sqrt{\left(\frac{\Delta_1 - \Delta_2}{2}\right)^2 + 2\Delta_3^2} \tag{7}$$

$$\alpha = \frac{E_2}{\sqrt{E_2^2 + 2\Delta_3^2}} \tag{8}$$

$$\beta = \frac{\sqrt{2}\Delta_3}{\sqrt{E_2^2 + 2\Delta_3^2}} \tag{9}$$

The states identification were made as described in Ref. [24]: HH (heavy hole) states are composed only by $|c_1\rangle$ or $|c_4\rangle$, LH (light hole) states are composed mainly of $|c_2\rangle$ or $|c_5\rangle$ and CH (crystal-field split-off hole) are composed mainly of $|c_3\rangle$ or $|c_6\rangle$. According to the identification of the energies presented in table I, E_1 is the HH state and, if $\alpha > \beta$, E_2 is the LH state and E_3 is the CH state or E_2 is the CH state and E_3 is the LH state otherwise. The valence band ordering in the Γ point, which depends on the values of Δ_1, Δ_2 and Δ_3, and the value of the coefficients for both crystal structures can be found in table II.

	Energies	α	β
ZB	$E_1 = E_2 > E_3$	0.57735	0.81650
WZ	$E_1 > E_2 > E_3$	0.98345	0.18116

Table II. The energy ordering and the α and β coefficients. The knowledge of these coefficients enable the identification of the states.

ZB identification	WZ identification
HH	HH
LH	CH
SO	LH

Table III. The WZ identification for the ZB states.

Since in our model we are using the WZ basis to describe the ZB structure it is useful to think that ZB is a WZ structure with zero crystal-field energy. Noting this feature we can identify the ZB valence band states in the Γ point using the WZ identification. This helps us to understand the band edge in the WZ/ZB interface in a quantum well structure. Table III relates the two different identifications.

As the dimensions of NWs are big enough to avoid lateral confinement, this structure can be considered as a 2-dimensional system, like a quantum well or a superlattice. In this context, we simulated a single WZ/ZB/WZ polytypic quantum well with 160Å well width and 320Å barrier width so that the whole system has 480Å.

Using the band mismatch value given in Ref. [19] it is possible to construct the quantum well profile. To understand the confinement profile we plotted, in figure 4a, the band edge energy in the WZ/ZB interface. Since the composition of the states LH and CH is different in both crystal structures we did not think it was convenient to draw a line connecting the energies. We believe that there's a mix of these values to form the effective potential. However, we can note that the conduction band and the first valence band form a type-II homostructure.

It is also convenient to plot the diagonal terms of the total Hamiltonian to check the variation of the parameters along the growth direction, which can be found in figure 4b. Although the nondiagonal terms of the matrix will mix the three profiles we can expect that the confinement of the electrons will be in the ZB region while the holes will be in the WZ region belonging in their most to the HH state.

The band structure of the quantum well plotted up to 10% of the k_x direction and 100% of the k_z direction is shown in figure 5. We can observe that the bound states in the valence band are mainly HH states, which means

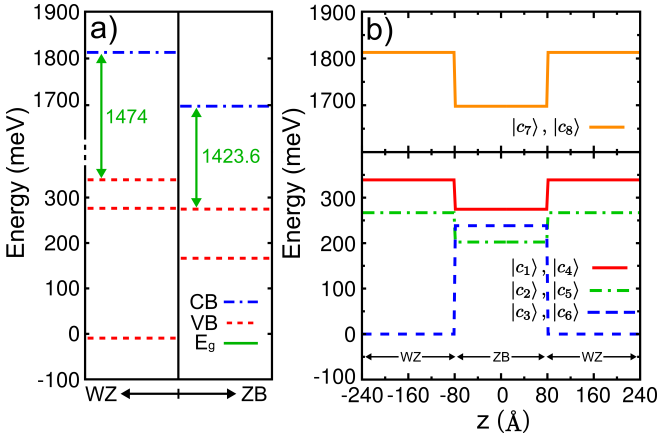


Figure 4. (a) The band edge energy in the WZ/ZB interface relating the WZ and ZB states. (b) The diagonal potential profile of the total Hamiltonian along the growth direction.

they are composed entirely by the $|c_1\rangle$ and $|c_4\rangle$ states of the basis that have only $|X\rangle$ and $|Y\rangle$ components. This feature directly reflects in the luminescence properties of the system: the light will be almost fully polarized in the xy plane, i. e., transversal to the growth axis of the polytypic quantum well. The LH states have less than 5% of $|Z\rangle$ component.

The probability densities calculated from the envelope functions for the Γ point of the EL1, EL2, EL3, HH1, HH2 and HH3 bands are shown in figure 6. These results agrees with the experimental data suggesting a spatial separation of the carriers, due to the fact that is more likely to find holes in the WZ region and electrons in the ZB region.

In a quantum well the selection rules for dipole optical transition are given by the matrix element M [25].

$$M = \langle E\,|\vec{r}\cdot\hat{\varepsilon}|\,H\rangle = M_c M_g \tag{10}$$

This matrix element can be divided in two parts: M_c and M_g. M_c is the matrix element between the electron and hole states in the basis $\{|c_l\rangle\}$ that depends on the polarization of the light and M_g is the overlap integral between the electron and hole envelope functions.

$$M_c = \langle c_e\,|\vec{r}\cdot\hat{\varepsilon}|\,c_h\rangle \tag{11}$$

$$M_g = \int_{-\infty}^{\infty} g_e^*(z)\, g_h(z)\, dz \tag{12}$$

The M_c matrix elements are known from symmetry properties of the Γ point and the non-vanishing elements are $\langle S\,|x|\,X\rangle$, $\langle S\,|y|\,Y\rangle$ and $\langle S\,|z|\,Z\rangle$. We just have to calculate the overlap integral M_g. Since the potential profile is even, the envelope functions have well defined parities, they are either even or odd and we can expect to have null overlap integrals between conduction and valence states. The non-zero overlap integrals and the difference energy in the Γ point are presented in table IV.

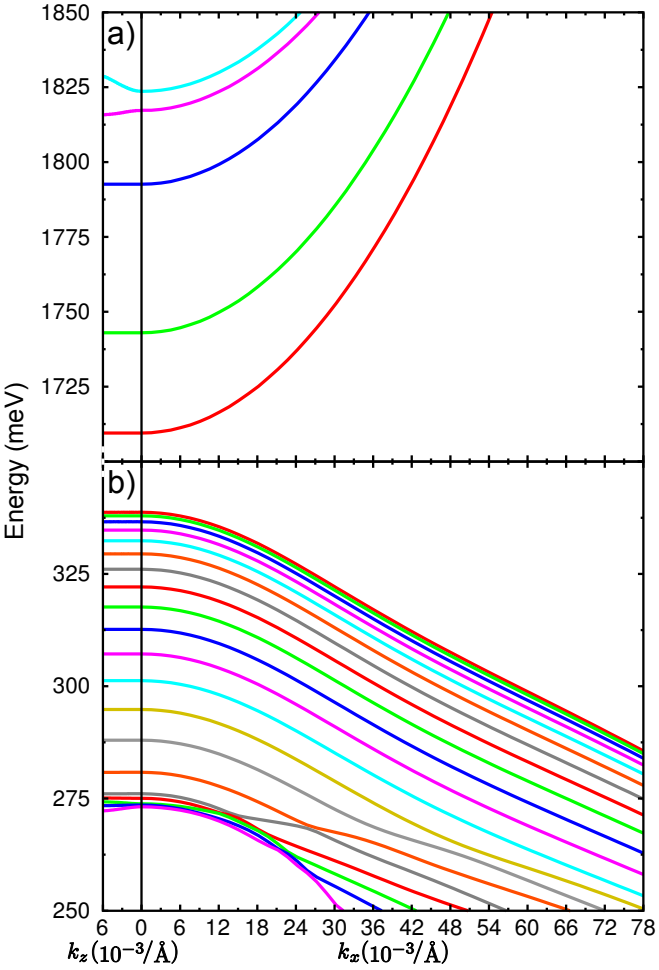


Figure 5. Conduction (a) and valence (b) band structure of the single WZ/ZB/WZ polytypic quantum well. From bottom to top the conduction band states are: EL1 - EL5. From top to bottom the valence band states are: HH1 - HH15, LH1, LH2, HH16, LH3, HH17.

	M_g (%)	Energy difference (meV)
EL1-HH1	∼2.6	1370.76
EL1-HH3	∼6.4	1372.89
EL2-HH2	∼12	1405.06
EL3-HH1	∼23	1453.86
EL3-HH3	∼33.5	1455.99

Table IV. Finite overlap integrals (M_g) and energy difference between some conduction and valence band states at the Γ point. We can note that overlap is bigger for excited states.

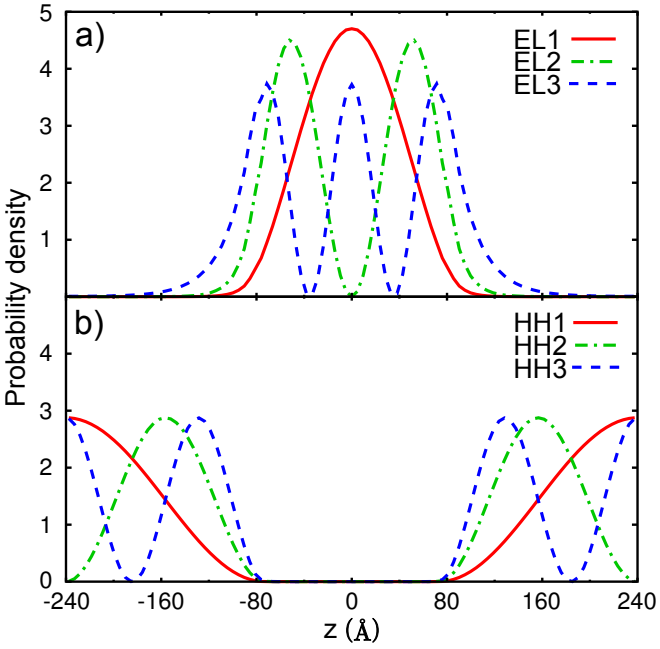


Figure 6. The probability densities of the electrons (a) and holes (b). We can note the spatial separation of the carriers.

Although we have achieved reliable results with the model considered here for InP, we believe that improvements should be made to treat other III-V compounds. In systems where the lower conduction band has symmetry Γ_7 in the WZ phase and the spin-orbit splitting is bigger or equivalent to the gap energy (InAs and InSb [19]) the full 8×8 $\vec{k}\cdot\vec{p}$ method should be considered with the inclusion of the Kane interband momentum matrix elements (P) and also Kane quadratic terms (B). In systems with Γ_8 symmetry in the lower conduction band for WZ phase, like AlAs or GaAs [19], the full symmetry analysis should be redone.

CONCLUSIONS

In summary, we have presented a theoretical method based in group theory arguments and the $\vec{k}\cdot\vec{p}$ method to calculate the electronic properties of InP polytypic structures in the vicinity of the band edges.

Understanding the behavior of the band structure of the calculated system we could predict the trends in the luminescence energy transitions. The preliminary results are in good agreement with the experimental data available so far such as carriers' spatial separation and light polarization in luminescence spectra.

With the proposed model, it will be possible to predict the optical properties of selected structures and to design systems that best fit new device applications.

ACKNOWLEDGEMENTS

We like to thank the Brazilian funding agencies CAPES and CNPq for the financial support.

[1] J. Bao, D. C. Bell, F. Capasso, N. Erdman, D. Wei, L. Froberg, T. Martensson, and L. Samuelson, Advanced Materials, **21**, 3654 (2009).
[2] J. Johansson, L. S. Karlsson, C. P. T. Svensson, T. Mårtensson, B. A. Wacaser, K. Deppert, L. Samuelson, and W. Seifert, Journal of Crystal Growth, **298**, 635 (2007).
[3] J. Johansson, L. S. Karlsson, C. P. T. Svensson, T. Martensson, B. A. Wacaser, K. Deppert, L. Samuelson, and W. Seifert, Nature Materials, **5**, 574 (2005).
[4] P. Caroff, K. A. Dick, J. Johansson, M. E. Messing, K. Deppert, and L. Samuelson, Nature Nanotechnology, **4**, 50 (2009).
[5] M. Tchernycheva, G. E. Cirlin, G. Patriarche, L. Travers, V. Zwiller, U. Perinetti, and J.-C. Harmand, Nano Letters, **7**, 1500 (2007).
[6] Y. Kitauchi, Y. Kobayashi, K. Tomioka, S. Hara, K. Hiruma, T. Fukui, and J. Motohisa, Nano Letters, **10**, 1699 (2010).
[7] S.-G. Ihn, J.-I. Song, Y.-H. Kim, J. Y. Lee, and I.-H. Ahn, Nanotechnology, IEEE Transactions on, **6**, 384 (2007).
[8] R. S. Wagner and W. C. Ellis, Applied Physics Letters, **4**, 89 (1964).
[9] V. Dubrovskii, G. Cirlin, and V. Ustinov, Semiconductors, **43**, 1539 (2009).
[10] F. Glas, Journal of Applied Physics, **104**, 093520 (2008).
[11] K. Sano, T. Akiyama, K. Nakamura, and T. Ito, Journal of Crystal Growth, **301-302**, 862 (2007).
[12] T. Akiyama, K. Sano, K. N. Akamura, and T. Ito, Japanese Journal of Applied Physics, **45**, L275 (2006).
[13] M. D. Moreira, P. Venezuela, and R. H. Miwa, Nanotechnology, **21**, 285204 (2010).
[14] N. Sibirev, M. Timofeeva, A. Bol′shakov, M. Nazarenko, and V. Dubrovskii, Physics of the Solid State, **52**, 1531 (2010).
[15] A. Nastovjak, I. Neizvestny, I. Shwartz, and Z. Yanovitskaya, Semiconductors, **44**, 127 (2010).
[16] M. Lubov, D. Kulikov, and Y. Trushin, Technical Physics Letters, **35**, 99 (2009).
[17] E. G. Gadret, G. O. Dias, L. C. O. Dacal, M. M. de Lima Jr., C. V. R. S. Ruffo, F. Iikawa, M. J. S. P. Brasil, T. Chiaramonte, M. A. Cotta, L. H. G. Tizei, D. Ugarte, and A. Cantarero, Physical Review B, **82**, 125327 (2010).
[18] M. Murayama and T. Nakayama, Phys. Rev. B, **49**, 4710 (1994).
[19] A. De and C. E. Pryor, Physical Review B, **81**, 155210 (2010).
[20] I. Vurgaftman, J. R. Meyer, and L. R. Ram-Mohan, Journal of Applied Physics, **89**, 5815 (2001).
[21] E. O. Kane, *Physics of III-V compounds vol. 1*, edited by R. K. Willardson and A. C. Beer, Semiconductors and Semimetals, Vol. 1 (World Scientific, 1966) Chap. 3, pp. 75–100.

[22] S. L. Chuang and C. S. Chang, Physical Review B, **54**, 2491 (1996).

[23] S. H. Park and S. L. Chuang, Journal of Applied Physics, **87**, 353 (2000).

[24] S. L. Chuang and C. S. Chang, Applied Physics Letters, **68**, 1657 (1996).

[25] M. Fox, *Optical Properties of Solids*, Oxford Master Series in Condensed Matter Physics (Oxford University Press, c2001) Chap. 6, pp. 115–142.